Experimental and numerical study on the shrinkage-deformation of carrot slices during hot air drying

Dalong Jiang[1†], Congcong Li[2,3*], Zifan Lin[4†], Yuntian Wu[5], Hongjuan Pei[6], Magdalena Zielinska[7], Hongwei Xiao[8]

(1. *School of Computer and Control Engineering, Yantai University, Yantai 264005, Shandong, China*;
2. *Hebei Agricultural University, Baoding 071001, Hebei, China*;
3. *Hebei Key Laboratory of Agricultural Big Data, Baoding 071001, Hebei, China*;
4. *Department of Electrical and Electronic Engineering, University of Western Australia, Perth 6000, Australia*;
5. *BeiGene Guangzhou Biologics Manufacturing Co., Ltd, Guangzhou 510555, China*;
6. *Neuroscience and Intelligent Media Institute, Communication University of China, Beijing 100024, China*;
7. *Department of Systems Engineering, University of Warmia and Mazury*, *Olsztyn 004889, Poland*;
8. *College of Engineering, China Agricultural University, Beijing 100083, China*)

Abstract: In order to further understand the mechanism of material volume change in the drying process, numerical simulations (considering or neglecting shrinkage) of heat and mass transfer during convective drying of carrot slices under constant and controlled temperature and relative humidity were carried out. Simulated results were validated with experimental data. The results of the simulation show that the Quadratic model fitted well to the moisture ratio and the material temperature data trend with average relative errors of 5.9% and 8.1%, respectively. Additionally, the results of the simulation considering shrinkage show that the moisture and temperature distributions during drying are closer to the experimental data than the results of the simulation disregarding shrinkage. The material moisture content was significantly related to the shrinkage of dried tissue. Temperature and relative humidity significantly affected the volume shrinkage of carrot slices. The volume shrinkage increased with the rising of the constant temperature and the decline of relative humidity. This model can be used to provide more information on the dynamics of heat and mass transfer during drying and can also be adapted to other products and dryers devices.

Keywords: carrot drying, numerical simulation, heat and mass transfer, shrinkage
DOI: 10.25165/j.ijabe.20231601.6736

Citation: Jiang D L, Li C C, Lin Z F, Wu Y T, Pei H J, Zielinska M, et al. Experimental and numerical study on the shrinkage-deformation of carrot slices during hot air drying. Int J Agric & Biol Eng, 2023; 16(1): 260–272.

1 Introduction

Fruits and vegetables are the daily necessities for everyone to eat, and their cellular structure is composed of about 80%-90% water[1]. Carrot is a highly perishable crop easy to deteriorate during postharvest handling and storage due to the relatively high moisture content[1]. Therefore, an appropriate processing method is required to extend its shelf life and availability throughout the whole year[2,3].

Drying is one of the most frequently used preservation techniques in the agricultural and food industries. Hot air drying is the most widely used method for the preservation of food in the processing industry[1]. Heat transfer occurs inside the sample by conduction and mass transfer takes place by diffusion in accordance with temperature and moisture concentration gradient[1,4]. Transport of water from the cellular structure to the surrounding may cause significant deformation of the material and irregular volume changes of high-moisture food products during drying. The reduction in the volume of dried particles can be defined as material shrinkage[1,5].

Shrinkage of dried products may negatively influence the quality of fruits and vegetables, i.e. mechanical and textural properties, and then consumer satisfaction[6]. For example, the changes in torsional stiffness (0.5 MPa to 7.0 MPa) of apples are related to the changes in the material shrinkage[7]. Shrinkage may also result in surface cracking and a reduction of the rehydration capability of dried products[8]. Moreover, it is an important factor that may affect drying kinetic and drying rate. Therefore, shrinkage should be taken into consideration while predicting heat and mass transfer processes[9,10].

Mathematical models are essential to predict and simulate the behavior of food products during drying. A number of mathematical models have been developed to predict heat and mass transfer in various food products subjected to different drying processes conducted in different configurations of dryers[11-14]. However, models that have been used to describe the drying of

Received date: 2021-05-02 **Accepted date:** 2021-11-27
Biographies: Dalong Jiang, PhD, research interest: intelligent drying equipment research and development, Email: 3473972630@qq.com; **Zifan Lin**, PhD candidate, research interest: power electronics, embedded system and microgrids, Email: zifan.lin@uwa.edu.au; **Yuntian Wu**, Bachelor, research interest: digital system, pharmaceutical, bio-chemistry, Email: yuntian.wu@beigene.com; **Hongjuan Pei**, PhD candidate, research interest: data mining, social networks, intelligent multimedia, Graph Representation Learning, machine learning and knowledge graph, Email: hjpei@cuc.edu.cn; **Magdalena Zielinska**, PhD, Associate Professor, research interest: quality control during processing and storage of agricultural products, research and development of new technology and equipment for energy saving and environmental protection drying, Email: m.zielinska@uwm.edu.pl; **Hongwei Xiao**, PhD, Associate Professor, research interest: agricultural product processing technology, Email: xhwcaugxy@163.com.
†These authors contributed equally to this study.
***Corresponding author: Congcong Li**, PhD, Associate Professor, research interest: intelligent information detection and processing. College of Information Science and Technology, Hebei Agricultural University, Baoding 071001, Hebei, China. Tel: +86-15033233222, Email: hebaulcc@126.com.

agri-food products were developed, to a large extent, without considering the volumetric shrinkage of food products during drying. For example, Yu et al.[1] reported that numerical simulations of heat and mass transfer were performed to investigate the hot air drying behavior of carrot cubes. However, he ignored the effect of material shrinkage on heat and mass transfer, which made it impossible to accurately simulate the drying process. The model predicting shrinkage and simultaneous heat and mass transfer in potatoes have been reported in literatures [15,16]. However, it considered food structure as compact and continuous, having negligible porosity. Also, some theoretical models developed based on some simplified assumptions have been used in the literature to describe the drying of food products[17,18]. The assumptions taken into consideration may simplify the problem formulation, but they are not conducive to solving a problem.

Some scholars have devoted themselves to studying the influence of shrinkage on the structure and heat and mass transfer of materials during the drying process because of its great significance. Segura et al.[19] reports on the numerical and experimental study on structural deformation of apple slices during heat and mass transfer processes. The results of simulations showed that the mathematical models of heat-mass transfer and stress-strain can be used to simulate effectively the hot-air drying of apple slices[19]. Also, the diffusive-convective model considering the shrinkage of pears provided a realistic and physical interpretation of the drying operation[20]. Tao et al.[21] found the change of heat and mass transfer pathways due to sample shrinkage was considered in the heat and mass transfer model.

Mathematical modeling of the drying processes may provide better insights into the shrinkage that accompanies simultaneous heat and mass transfer processes. However, limited studies have been conducted on the empirical modeling of the shrinkage of fruits and vegetables. In-depth understanding of the mechanism of structural deformation of agri-food products is crucial for the optimization of hot air drying parameters as well as for obtaining high-quality dried vegetables. As above, it is highly recommended to investigate the mechanism of shrinkage-deformation of carrot slices that accompanies simultaneous heat and mass transfer processes. Therefore, the objectives of this study were to 1) determine the effect of different drying conditions on the shrinkage-deformation of carrot slices; 2) study the effect of shrinkage on the simultaneous heat and mass transfer processes; 3) model heat and mass transfer processes during convective drying of carrot slices in a fully coupled manner using COMSOL Multiphysics.

2 Materials and methods

2.1 Materials

Fresh carrots (*Daucus carota* L.) were purchased from Qinghe Vegetable Market, Beijing. All samples were stored in a refrigerator at 4°C and 90% relative humidity before experiments. Carrots were peeled and diced into cylinders with a diameter of 0.033 m and thickness of 0.004 m, 0.006 m, 0.008 m, and 0.010 m. The initial moisture content of carrot slices was 90.3%±0.5%. The initial moisture content of carrot slices was measured by the oven atmospheric drying method[22].

2.2 Drying system

Hot air drying experiments were performed in laboratory-scale hot air drying equipment installed in the College of Engineering of China Agricultural University, Beijing, China. A schematic diagram of the dryer, which was previously described by Yu et al.[1] is shown in Figures 1a and 1b. The dryer consisted mainly of electric heating tubes to heat the inlet air; axial flow fans to blow air into the drying chamber and ensure uniformity of airflow; a centrifugal fan to remove humid air from the drying chamber; a control system and shell; and a humidifier to increase the RH of the drying air. Significantly, there are large pores at the bottom of the plastic tray to ensure that the bottom and top surfaces of the materials are consistent during the drying process, mass transfer, convective, and evaporation on the bottom of carrot slices can occur simultaneously.

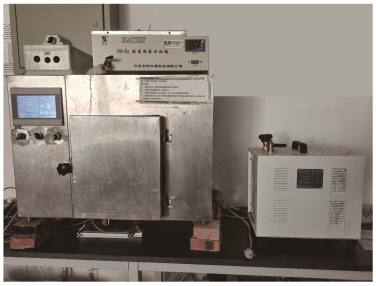

a. Experimental apparatus

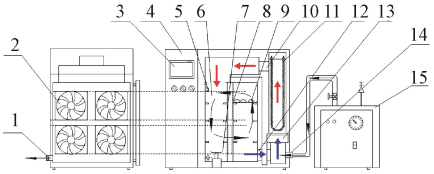

1. Dehumidification fan 2. Turbulence fan 3. Human-machine interface 4. Power distribution cabinet 5. Pt100 temperature sensor 6. Drying chamber 7. weighing module 8. Plastic tray 9. Material 10. Inlet air pipe 11. Finned heating tube 12. Return air pipe 13. Forced draft fan 14. Air inlet 15. Superheated steam generator.

b. Schematic diagram

Figure 1 A lab-scale convective dryer with hot-air circulation

Since the verification was performed via thin layer drying using trays, it was unable to maintain the RH value at a high level by water evaporation from materials, especially in the later period. The apparatus adopted a humidifier on the right of the experimental equipment to make sure constant RH values (Figure 1a). The humidifier operation and the exhaust fan were coordinated to keep the RH value at constant value[1].

2.3 Experimental procedure

The temperature of carrot slices in the thin layers was monitored using a temperature sensor (PT100, TD Sensors Technology, China) every 2 s with an accuracy of ±0.3°C[1]. The temperature sensor (needle-shaped probe with a diameter of 0.002 m and a length of 0.010 m) was inserted into a sample at different locations. The mass of samples was measured using an automatic weighting system (Beijing Kang Sen technology co. LTD, China) every 1200 s with an accuracy of (0.320±0.01) kg[1]. The RH of the drying medium in the drying chamber was monitored using a type of sensor (SHT75, Switzerland) with an accuracy of ±1.8%. The air velocity in the drying chamber was measured using a meter (TESTO 435-3, Testo SE & Co., KgaA, Germany) with an accuracy of ±0.03 m/s. The mass and temperature changes of carrot slices were used for model validation[1]. The high-performance digital camera was used for image capture of carrot slices from different angles every 1200 s. The thickness and diameter information extracted from the captured images was analyzed using MATLAB R2016b software (MathWorks Corporation, America) and then the shrinkage of carrot slices was determined by an industrial camera (ACA250014-GC, Basler, Germany)[23]. Due to the obvious difference between the material surface color and the

background color, the size of the image taken by the vision system can be calculated by using the pixels. All the experiments were carried out in triplicate and the average value was used for further analysis. A complete graphing and data analysis software package Origin Pro 2015 (OriginLab Corporation, America) was used for data analysis. The experimental parameters are given in Table 1.

Table 1 Experimental design and parameters

Experiment	T/°C	RH/%	TH/m
1	60	20	0.004
2	60	20	0.006
3	60	20	0.008
4	60	20	0.010
5	50	20	0.006
6	70	20	0.006
7	80	20	0.006
8	60	30	0.006
9	60	40	0.006
10	60	50	0.006

Note: T: Temperature, °C; RH: Relative humidity, %; TH: Sample thickness, m.

The moisture content (M_t) was calculated as follows[1]:

$$M_t = \frac{W_t - G}{g} \tag{1}$$

where, M_t indicates the moisture content at any time, kg/kg d.b. (dry base); W_t indicates the material mass at any time, kg; G indicates the mass of a dry matter, kg.

Moisture ratio (MR) was calculated from the following equation[1]:

$$\mathrm{MR} = \frac{M_t}{M_0} \tag{2}$$

where, M_0 indicates the initial moisture content, kg/kg d.b. (dry basis); M_t indicates the moisture content at any time t, kg/kg d.b.

The thickness shrinkage SR_t was calculated according to Equation (3).

$$\mathrm{SR}_t = \frac{\mathrm{TH}_0 - \mathrm{TH}_t}{\mathrm{TH}_0} \tag{3}$$

where, SR_t indicates the thickness shrinkage; TH_t indicates the sample thickness at any time t during drying, m; TH_0 indicates the initial sample thickness, m.

The cross-sectional shrinkage SR_d was calculated as follows:

$$\mathrm{SR}_d = \frac{d_0 - d_t}{d_0} \tag{4}$$

where, SR_d indicates the cross-sectional shrinkage; d_t indicates the cross-sectional diameter of the sample at any time t, m; d_0 indicates the initial cross-section diameter of a sample, m.

The volume shrinkage SR_v was calculated as follows:

$$\mathrm{SR}_v = 1 - \frac{d_t^2 \mathrm{TH}_t}{d_0^2 \mathrm{TH}_0} \tag{5}$$

where, SR_v indicates the volume shrinkage, %; d_t indicates the cross-sectional diameter of the sample at any time t, m; d_0 indicates the initial cross-section diameter of a sample, m; TH_t indicates sample thickness at any time t during drying, m; TH_0 indicates the initial sample thickness, m.

The rate of thickness shrinkage SRR_t was calculated as follows:

$$\mathrm{SRR}_t = \frac{\mathrm{SR}_{tt1} - \mathrm{SR}_{tt2}}{t_2 - t_1} \tag{6}$$

where, t_1 and t_2 indicates drying time, s; SR_{tt1}, SR_{tt2} indicate the thickness shrinkage at drying time of t_1 and t_2, %; SRR_t indicates the rate of thickness shrinkage, 1/s.

The rate of cross-sectional shrinkage as well as the rate of volume shrinkage were calculated as follows:

$$\mathrm{SRR}_d = \frac{\mathrm{SR}_{dt1} - \mathrm{SR}_{dt2}}{t_2 - t_1} \tag{7}$$

$$\mathrm{SRR}_V = \frac{\mathrm{SR}_{Vt1} - \mathrm{SR}_{Vt2}}{t_2 - t_1} \tag{8}$$

where, SR_{dt1}, SR_{dt2} indicate the cross-sectional shrinkage at the drying time t_1 and t_2, %; SR_{Vt1}, SR_{Vt2} indicate the volume shrinkage at the drying time t_1 and t_2, %; SRR_d and SRR_V indicate the rate of cross-sectional shrinkage and the rate of volume shrinkage, respectively, 1/s.

The shrinkage isotropy parameter was defined as the ratio of thickness shrinkage to diameter shrinkage. A shrinkage isotropy parameter close to 1 indicates uniform shrinkage of carrot slices during drying. Unit volume dehydration was defined as the ratio of volume at the drying time t to the initial material volume.

2.4 Model development

2.4.1 Physical model and assumptions

The schematic domain of the heat and mass transfer model was shown in Figure 2. The 2D axisymmetric cylindrical geometry has been considered for the computational domain. The radius and thickness of the cylinder were r=0.033 m and TH=0.006 m, respectively. The model was discretized into the structured mesh with 3700 triangular elements.

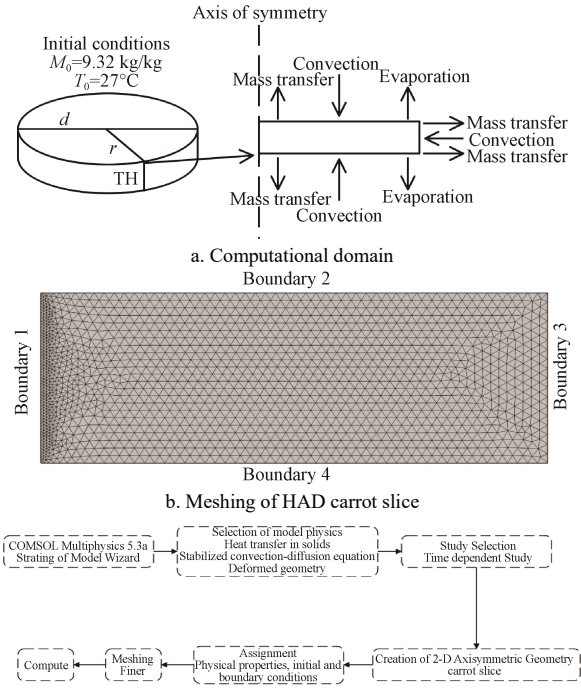

Figure 2 Computational domain, meshing of HAD carrot slice, and flow chart showing model development strategy in COMSOL software

Based on Fourier's law and Fick's second law, the transient 3D temperature and moisture content distributions in the carrot slice were computed[1]. The following assumptions have been made to simplify modeling and analysis of the drying of carrot slices: 1) hot air transferred heat by the convection; 2) there was no heat exchange between the drying chamber and the external environment; 3) the moisture transfer in the sample was carried out by diffusion; 4) water was transferred from the center to the material surface in the liquid state and then evaporated; 5) the

moisture content in the sample was evenly distributed in the early stages of drying; 6) the heat transfer from the surface to the interior of the sample took place through the conduction; 7) the changes in the shrinkage rate were described by the quadric equation[1,24].

2.4.2 Mathematical formulation

The governing equation of mass transfer during drying can be given as follows[1,25]:

$$\frac{\partial M}{\partial t}=\frac{\partial}{\partial r}\left(D_{\text{eff}}\frac{\partial M}{\partial r}\right)+\frac{\partial}{\partial h}\left(D_{\text{eff}}\frac{\partial M}{\partial h}\right) \tag{9}$$

with the following initial and boundary (2, 3, 4) conditions[1]:

$$M\left(t=0\right)=M_0 \tag{10}$$

$$-\rho D_{\text{eff}}\frac{\partial M}{\partial r}=h_m\left(\text{WC}_m-\text{WC}_{air}\right) \tag{11}$$

$$-\rho D_{\text{eff}}\frac{\partial M}{\partial h}=h_m\left(\text{WC}_m-\text{WC}_{air}\right) \tag{12}$$

where, M indicates the moisture content, kg/kg, d.b.; D_{eff} indicates the effective moisture diffusivity of the material, m^2/s; ρ indicates the density of carrot slice, kg/m^3; t indicates drying time, s; r and h indicate the coordinates of the point at which the coordinates intersect the model face vertically, m; WC_{air} indicates the concentration of water vapor in the hot air, kg/m^3; WC_m indicates the concentration of water vapor at the material surface, kg/m^3; h_m indicates the mass transfer coefficient, m/s.

The governing equation of heat transfer during drying can be given as follows[1]:

$$\rho C_p\frac{\partial Tm}{\partial t}=\frac{\partial}{\partial r}\left(k\frac{\partial Tm}{\partial r}\right)+\frac{\partial}{\partial h}\left(k\frac{\partial Tm}{\partial h}\right)+\rho_w r_w\frac{\partial M}{\partial t} \tag{13}$$

Considering the relatively small value of latent heat of water evaporation at Boundaries 2, 3, and 4, the above equation was usually simplified into Equation (14):

$$\rho C_p\frac{\partial Tm}{\partial t}=\frac{\partial}{\partial r}\left(k\frac{\partial Tm}{\partial r}\right)+\frac{\partial}{\partial h}\left(k\frac{\partial Tm}{\partial h}\right) \tag{14}$$

$$T_m\left(t=0\right)=T_0 \tag{15}$$

$$h_t\left(T_{air}-T_m\right)=k\frac{\partial T}{\partial r}-r_w h_m\left(WC_m-WC_{air}\right) \tag{16}$$

$$h_t\left(T_{air}-T_m\right)=k\frac{\partial T}{\partial h}-r_w h_m\left(WC_m-WC_{air}\right) \tag{17}$$

where, C_p indicates the specific heat of material, J/kg·K; T_m indicates material temperature, K; T_0 indicates the initial temperature of the material, K; k indicates thermal conductivity of material, W/m·K; T_{air} indicates the temperature of hot air, K; h_t indicates the heat transfer coefficient, $W/m^2\cdot K$; r_w indicates the latent hewat of water vaporization, J/kg; ρ_w indicates the water density, kg/m^3.

The heat (h_t) and mass (h_m) transfer coefficients for convection were estimated by Chilton and Colburn analogy[1,26,27]:

$$\text{Nu}=2+0.552\,\text{Re}^{0.53}\,\text{Pr}^{1/3} \tag{18}$$

$$\text{Sh}=2+0.552\,\text{Re}^{0.53}\,\text{Sc}^{1/3} \tag{19}$$

Where, Nu, Sh, Re, Pr, and Sc were the Nusselt, Sherwood, Reynolds, Prandtl, and Schmidt numbers.

The Nusselt, Sherwood, Reynolds, Prandtl, and Schmidt numbers were calculated using Equations (19)-(23)[1,28]:

$$\text{Nu}=\frac{\text{TH}_t d_E}{\lambda} \tag{20}$$

$$\text{Sh}=\frac{h_m d_E}{D_{AB}} \tag{21}$$

$$\text{Re}=\frac{d_E v\rho^{air}}{\mu_{air}} \tag{22}$$

$$\text{Pr}=\frac{C_{p,air}\mu_{air}}{\lambda} \tag{23}$$

$$\text{Sc}=\frac{\mu_{air}}{\rho_{air}D_{AB}} \tag{24}$$

where, d_E indicates the average diameter of the volume of carrot slice, m; D_{AB} indicates diffusivity of water vapor in the air, m^2/s; v indicates air velocity, m/s; λ indicates thermal conductivity of air, W/m·K; μ_{air} indicates dynamic viscosity of air, Pa·s; ρ_{air} indicates air density, kg/m^3; $C_{p,air}$ indicates specific heat of air, J/kg·K.

The drying medium was considered a mixture of independent gases, i.e. dry air and water vapor. The concentration of water vapor at the material surface (WC_m) was calculated according to the following equation[1,29]:

$$\text{WC}_m=\frac{2.1667}{1000}\times A_w\times\frac{P_s(T_m)}{T_m} \tag{25}$$

where, A_w indicates water activity; P_s indicates the saturated water vapor pressure at the sample surface, Pa.

Water activity was measured at the temperature of 60°C using a water activity meter (Aqualab, METER, USA) and related to the moisture content using the following polynomial equations[1]:

$$A_w=(-0.0007M^4+0.0141M^3-0.1016M^2+0.3189M+0.5972)\,|_{M>0.7} \tag{26}$$

$$A_w=(-182.92M^4+217.25M^3-97.06M^2+20.31M-1.0808)\,|_{M<0.7} \tag{27}$$

where, A_w indicates the water activity; M indicates the moisture content, kg/kg, d.b.

The saturated water vapor pressure at the sample surface was related to the temperature using the following formula[1,26]:

$$P_s=\exp\left(\frac{-5.8\times10^3}{T_s}+1.01-4.864\times10^{-2}T_s+4.176\times10^{-5}T_s^{\,2}-1.445\times10^{-8}T_s^{\,3}+6.546\ln T_s\right) \tag{28}$$

where, P_s indicates the saturated water vapor pressure at the sample surface, Pa; T_s indicates material surface temperature, K.

The concentration of water vapor in the hot air (WC_{air}) was calculated using the following equation[1,29]:

$$\text{WC}_{air}=\frac{2.1667}{1000}\times\frac{\text{RH}}{100}\times\frac{P_s(T_{air})}{T_{air}} \tag{29}$$

where, RH indicates the relative humidity of the drying air, %; P_s indicates the saturated water vapor pressure at the sample surface, Pa; T_{air} indicates the temperature of hot air, K.

The latent heat of water evaporation (r_w) was given by the following equation[1,26]:

$$r_w=2501.05\times10^3\times\left(\frac{647.3-T_s}{647.3-273.15}\right)^{0.3298} \tag{30}$$

where, r_w indicates the latent heat of water evaporation, J/kg; T_s indicates material surface temperature, K.

Considering the significant correlation between shrinkage and material moisture content, the experiment also showed that the relationship between shrinkage and moisture ratios was described by the equation:

$$\text{SR}=A+B\times\text{MR}+C\times(\text{MR})^2 \tag{31}$$

where, A, B, and C indicate the empirical parameter; MR indicates the moisture ratio; SR indicates the volume shrinkage ratio, %.

Since the shrinkage mainly occurs in the radial direction of the

material, therefore, the changes in the material radius with drying time were calculated as follows:

$$r(t) = r_0 \times \mathrm{SR} \tag{32}$$

where, $r(t)$ indicates the changes in material radius with drying time, (mm·%); r_0 indicates the initial material radius, m; t indicates the drying time, s.

Therefore, the dynamic change process of material shrinkage is further discretized into the shrinkage ratio of material during drying was calculated as follows:

$$v_{\mathrm{SR}} = \frac{\mathrm{d}r}{\mathrm{d}t} \tag{33}$$

where, v_{SR} indicates the shrinkage rate, m/s.

The thermophysical properties of carrots were calculated according to the formulas[1,28,30,31]:

$$\rho = 440.001 + 90M \tag{34}$$

$$C_p = 1750 + 2345\left(\frac{M}{M+1}\right) \tag{35}$$

$$k = 0.49 - 0.443\exp(-0.206M) \tag{36}$$

$$D_{\mathrm{eff}} = 2.78 \times 10^{-4} \exp\left(-0.97 - \frac{3459.8}{T_m} + 0.059M\right) \tag{37}$$

where, ρ indicates the density of carrot slices, kg/m^3; M indicates the moisture content of the material, kg/kg d.b.; C_p indicates the specific heat capacity of the material, J/kg·K; k indicates the material thermal conductivity, W/m·K; D_{eff} indicates the effective water diffusivity of material, m^2/s; T_m indicates the material temperature, K.

The software COMSOL Multiphysics 5.3a was used to simulate the heat and mass transfer processes during the hot air drying of carrot slices. The effect of shrinkage on the simultaneous heat and mass transfer processes was evaluated. The solid heat transfer module was used to solve the problem of heat transferred by the process of convection from hot air to the carrot slices and the temperature distribution within the examined carrot slices was evaluated. The moisture gradient was obtained using the Transport of the diluted species module of COMSOL. The shrinkage in diameter of carrot slices was evaluated using an arbitrary Lagrangian-Eulerian method and the deformation geometry module (Figure 2c). All the physical parameters required for simulations were obtained experimentally or from literature sources. Two different steps, i.e., 30 s and 120 s, were used as the initial and maximum values, respectively. COMSOL simulations were running using a 1.7 GHz Windows Lenovo workstation with an Intel Xeon CPU E5-2609, 1.70 GHz, 64 GB RAM, windows 10 (64 bit) operating system. A total running time was 600 s for an extra finer mesh consisting of 9012 domain elements (triangular).

2.4.3 Model validation

The thin layer drying models, i.e., Atamipour, Quadratic, Vazquez, and Exponential, were selected to fit the experimental data. The software 1stOpt (7D-Soft High Technology Inc., American) was used to fit the models to the experimental data.

2.5 Statistical analysis

The coefficient of determination (R^2) and root mean square error (RMSE) was selected as the evaluation indexes[32]:

$$R^2 = 1 - \frac{\sum_{i=1}^{N}(\mathrm{SR}_{\mathrm{pre},i} - \mathrm{SR}_{\mathrm{exp},i})^2}{\sum_{i=1}^{N}(\overline{\mathrm{SR}_{\mathrm{pre},i}} - \mathrm{SR}_{\mathrm{exp},i})^2} \tag{38}$$

$$\mathrm{RMSE} = \sqrt{\frac{\sum_{i=1}^{N}(\mathrm{SR}_{pre,i} - \mathrm{SR}_{\mathrm{exp},i})^2}{N}} \tag{39}$$

where, $\mathrm{SR}_{\mathrm{exp},i}$ indicates the i-th experimental shrinkage value, %; $\mathrm{SR}_{\mathrm{pre},i}$ indicates the i-th modeled shrinkage value, %; N indicates the number of measurements for moisture ratio; $\overline{\mathrm{SR}_{\mathrm{exp},i}}$ and $\overline{\mathrm{SR}_{\mathrm{pre},i}}$ indicate the mean values of experimental and predicted shrinkage, %, respectively.

The larger was R^2 value and the smaller was RMSE value, the better the fitting of the model[32].

The relative percent error (E) between calculated and experimental data was estimated by the following equation[9]:

$$E = \frac{100}{N}\sum_{i=1}^{N}\frac{\left|M_{\mathrm{exp},i} - M_{\mathrm{pre},i}\right|}{M_{\mathrm{exp},i}} \tag{40}$$

where, E indicates the relative percent error, %; $M_{\mathrm{exp},i}$ indicates the i-the experimental moisture content, kg/kg d.b.; $M_{\mathrm{pre},i}$ indicates the i-th modeled moisture content, kg/kg d.b.; N indicates the number of measurements for moisture ratio.

3 Results and discussion

3.1 The effect of sample thickness on the shrinkage of carrot slices

The volume shrinkage of carrot slices of different thicknesses increased with the drying time until they became stable (Figure 3a). In all cases studied, it became stable for values higher than 80%. The smaller the thickness of carrot slices was, the faster the volume shrinkage of the material to be dried. The reason for this can be the fact that the smaller the thickness of carrot slices was, the shorter the moisture migration path. A similar trend was observed in the case of thickness shrinkage and diameter shrinkage (Figures 3b and 3c). The thickness shrinkage of carrot slices of the thickness of 0.010 m increased significantly with the drying time up to 60%, while the diameter shrinkage of carrot slices of the thickness of 0.010 m increased significantly with the drying time up to 35%.

The shrinkage isotropy parameter fluctuated at the initial stage of drying, and then gradually tended to be stable. The rapid evaporation of moisture resulted in an uneven shrinkage in the early stages of drying. As the thickness shrinkage was significantly higher than the diameter shrinkage, the shrinkage isotropy parameter of carrot slices of the thickness of 0.010 m fluctuated significantly during drying. Much smaller fluctuations were observed in the case of the shrinkage isotropy parameter of carrot slices of the thickness of 0.006 m. Then, the sample thickness of 0.006 m was selected for the subsequent simulation of the drying process. Also, some additional assumptions have been made, i.e., 1) the sample diameter was significantly larger than the sample thickness; 2) the shrinkage fitting model did not consider the thickness shrinkage.

3.2 Effect of drying temperature and relative humidity on the shrinkage of carrot slices

The volume shrinkage of carrot slices increased even up to 80% with the drying time (Figure 4a). The volume shrinkage of carrot slices dried at the temperature of 50°C, 60°C, 70°C, and 80°C was 76.3%, 79.4%, 81.7%, and 83.7%, respectively. The results show that the drying temperature significantly influenced the volume shrinkage of carrot slices during drying. The higher the drying temperature in the early stage of drying and the higher

the difference in the capillary pressure, the faster the increase in the volume shrinkage of carrot slices was observed. The result is consistent with the literature data[26]. The volume shrinkage rate reached its highest peak at the beginning of the drying process, and then the shrinkage rate decreased gradually (Figure 4b). The results show that the collapse of pores due to the thermal stress led to significant deformation of the material to be dried. Additionally, it can be stated that the free water existing in the macropores was quite easy to remove, while the presence of associated water in the small pores could result in less deformation of the material tissue. The results are consistent with the literature data[27].

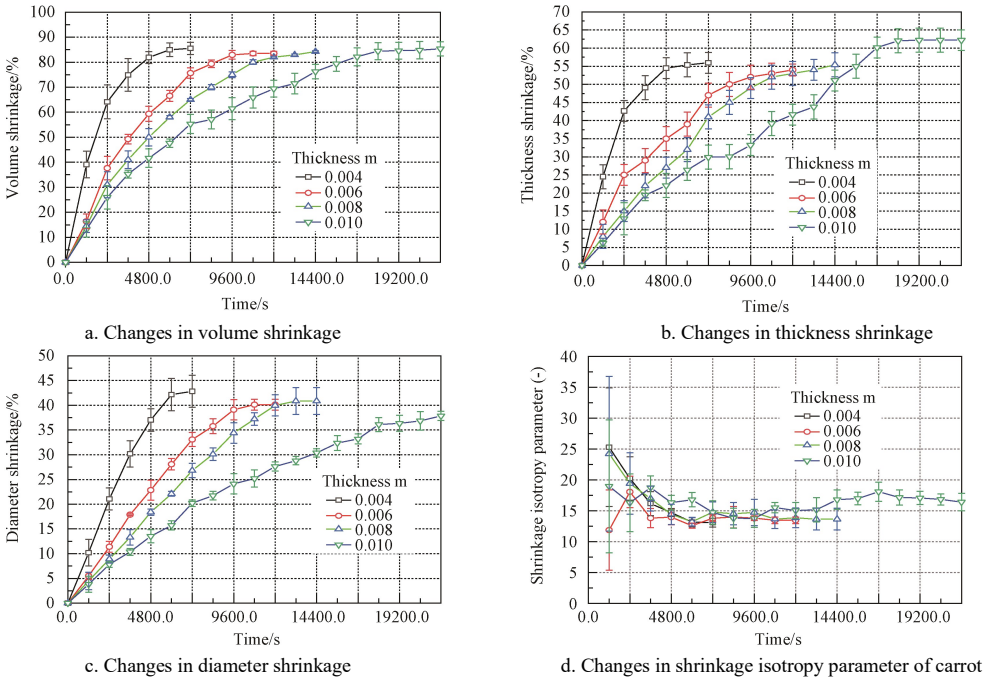

a. Changes in volume shrinkage b. Changes in thickness shrinkage

c. Changes in diameter shrinkage d. Changes in shrinkage isotropy parameter of carrot slices

Figure 3 Influence of sample thickness on the shrinkage of carrot slices during drying at the temperature of 60°C, air velocity of 0.3 m/s, and RH of 20%

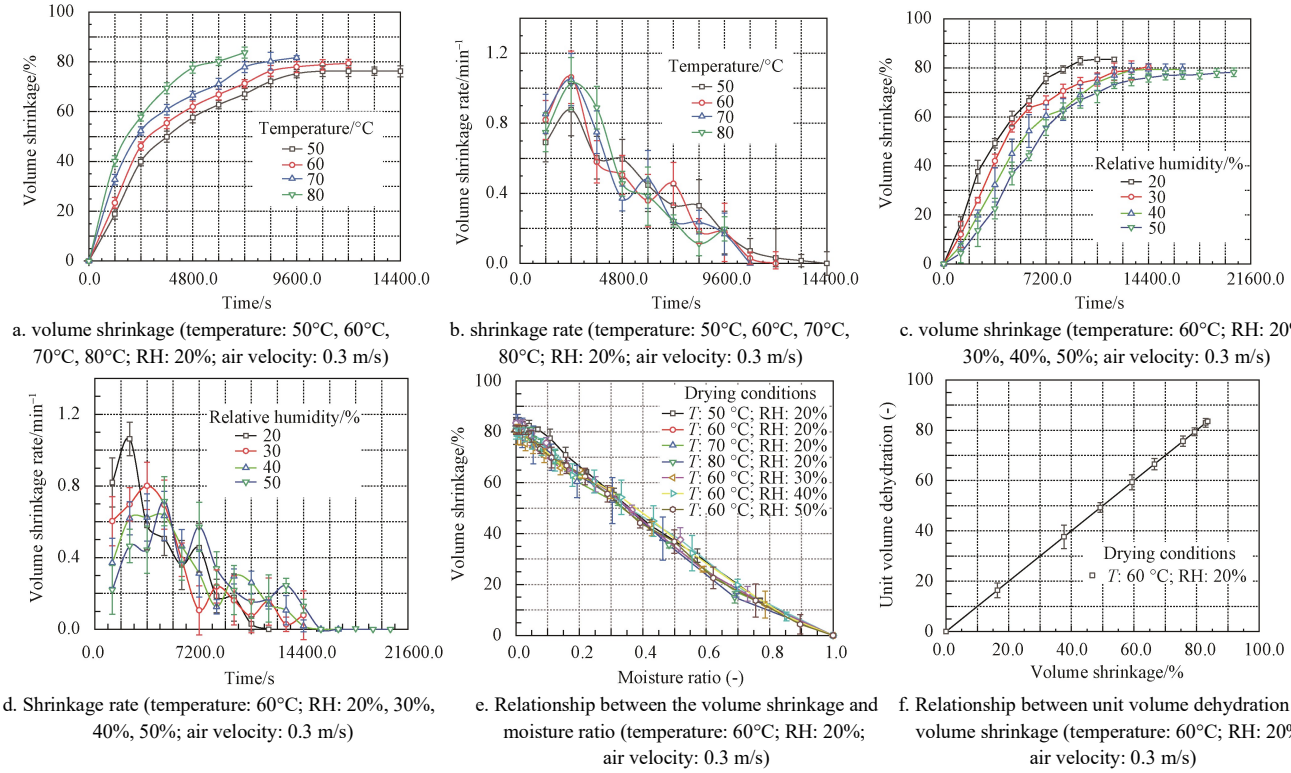

a. volume shrinkage (temperature: 50°C, 60°C, 70°C, 80°C; RH: 20%; air velocity: 0.3 m/s)

b. shrinkage rate (temperature: 50°C, 60°C, 70°C, 80°C; RH: 20%; air velocity: 0.3 m/s)

c. volume shrinkage (temperature: 60°C; RH: 20%, 30%, 40%, 50%; air velocity: 0.3 m/s)

d. Shrinkage rate (temperature: 60°C; RH: 20%, 30%, 40%, 50%; air velocity: 0.3 m/s)

e. Relationship between the volume shrinkage and moisture ratio (temperature: 60°C; RH: 20%; air velocity: 0.3 m/s)

f. Relationship between unit volume dehydration and volume shrinkage (temperature: 60°C; RH: 20%; air velocity: 0.3 m/s)

Figure 4 Influence of drying conditions on the volume shrinkage and shrinkage rate of carrot slices of the thickness of 6 mm during hot air drying

In the early stage of drying the shrinkage of carrot slices increased gradually with a decrease in the relative humidity of the drying air (Figure 4c). The volume shrinkage of carrot slices dried by the hot air of the relative humidity of 20%, 30%, 40%, and 50% was 83.49%, 80.53%, 79.39%, and 78.22%, respectively. The lower relative humidity of the drying medium which corresponded to the higher drying strength led to a greater shrinkage stress of material tissue during drying. The volume shrinkage rate of carrot slices decreased with an increase in the drying time (Figure 4d). The results show that the structure of the skeleton of carrot slices was formed and fixed in the early stage of drying. As a consequence, the moisture migration in the later stages of the

drying process did not damage the tissue structure of the carrot. The results are consistent with data published for apple slices[33].

The volume shrinkage linearly decreased with the decrease in moisture ratio of carrot slices dried under different drying conditions (Figure 4e). The results show that the changes in moisture content constitute the main factor affecting the volume shrinkage of carrot slices dried under different drying conditions. The linear relationship between volume shrinkage and dehydration rate per unit volume under the drying temperature of 60°C, air velocity of 0.3 m/s, relative humidity of 20%, and carrot slice thickness of 0.006 m was found to be significant (R^2=0.9980) (Figure 4f).

3.3 Shrinkage model fitting analysis

A significant correlation was found between volume shrinkage and moisture ratio under a constant relative humidity of 20% and different drying temperature (50°C, 60°C, 70°C, 80°C) or constant drying temperature of 60°C and different relative humidity (20%, 30%, 40%, 50%). In most cases, the values of the coefficient of determination (R^2) of the Hatamipour, Quadratic, and Vazquez models were higher than 0.99, while the values of the coefficient of determination of the Exponential model were lower than 0.99. The results confirm the usefulness of Hatamipour, Quadratic, and Vazquez models in the prediction of drying characteristics of carrot slices. Based on the results obtained in this study, the Quadratic model (including parameters such as *A*, *B*, *C*, and MR) was selected to simulate the relationship between volume shrinkage and moisture ratio under constant drying conditions (Tables 2 and 3).

Table 2 Model parameters and fitting degree under different drying temperatures

Model	*T*/°C	Parameters					R^2	RMSE
		A	B	C	D	E		
Hatamipour SR=A+B×MR	50	0.85	−0.89	--	--	--	0.9936	0.0221
	60	0.83	−0.87	--	--	--	0.9947	0.0200
	70	0.80	−0.85	--	--	--	0.9894	0.0283
	80	0.81	−0.87	--	--	--	0.9846	0.0341
Quadratic SR=A+B×MR+ C×MR^2	50	0.86	−1.06	0.19	--	--	0.9969	0.0152
	60	0.84	−1.03	0.18	--	--	0.9982	0.0113
	70	0.82	−1.11	0.28	--	--	0.9981	0.0119
	80	0.85	−1.20	0.34	--	--	0.9955	0.0182
Vazquez SR=A+B×MR+ C×(MR)$^{2/3}$+ D×exp(E×MR)	50	−5.33	0.80	0.69	6.16	−0.47	0.9994	0.0062
	60	0.84	−0.80	−0.10	1.20	36.24	0.9987	0.0097
	70	0.98	0.10	−1.10	−0.14	−10.68	0.9979	0.0125
	80	−105.58	9.94	0.81	106.37	−0.11	0.9963	0.0166
Exponential SR=A×exp(B×MR)	50	0.89	−1.88	--	--	--	0.9619	0.0563
	60	0.87	−1.88	--	--	--	0.9652	0.0538
	70	0.84	−1.99	--	--	--	0.9720	0.0486
	80	0.91	−2.16	--	--	--	0.9676	0.0522

Note: R^2 is the correlation coefficient-; RMSE is the root mean square error; A, B, C, D, and E were empirical coefficients of contraction.

Table 3 Model parameters and fitting degree under different relative humidity

Model	RH/%	Parameters					R^2	RMSE
		A	*B*	*C*	*D*	*E*		
Hatamipour SR=A+B×MR	20	0.83	–0.87	--	--	--	0.9947	0.0200
	30	0.79	–0.82	--	--	--	0.9939	0.0202
	40	0.80	–0.83	--	--	--	0.9967	0.0152
	50	0.81	–0.86	--	--	--	0.9944	0.0208
Quadratic SR=A+B×MR+ C×MR^2	20	0.84	–1.03	0.18	--	--	0.9983	0.0114
	30	0.80	–0.94	0.13	--	--	0.9956	0.0172
	40	0.81	–0.88	0.06	--	--	0.9971	0.0144
	50	0.82	–1.03	0.19	--	--	0.9944	0.0208
Vazquez SR=A+B×MR+ C×(MR)$^{2/3}$+ D×exp(E×MR)	20	1.23	–0.60	−0.26	−0.38	5.87	0.9972	0.0143
	30	–145.94	6.90	0.17	146.72	−0.05	0.9958	0.0168
	40	0.79	–0.95	0.09	1.06	15.62	0.9983	0.0107
	50	–89.64	6.95	0.34	90.44	−0.09	0.9983	0.0113
Exponential SR=A×exp(B×MR)	20	0.87	–1.88	--	--	--	0.9617	0.0538
	30	0.82	–1.85	--	--	--	0.9580	0.0558
	40	0.84	–1.82	--	--	--	0.9541	0.0593
	50	0.84	–1.95	--	--	--	0.9666	0.0534

3.4 Validation of a computational model

A grid independence study was performed under the present research to eliminate/reduce the influence of the number of grid sizes on the computational results. For this purpose, the influence of the number of cells on the computed (computations considered material shrinkage) moisture content and the temperature in the center of the carrot slice was evaluated. Through analyzing grid independence, the minimum number of grid cells needed to get grid-independent results were evaluated. The results tended towards identical when the number of cells increased from 5000.0 to 9124.0 (Figure 5). Therefore, the grid with 9124.0 cells was considered grid-independent.

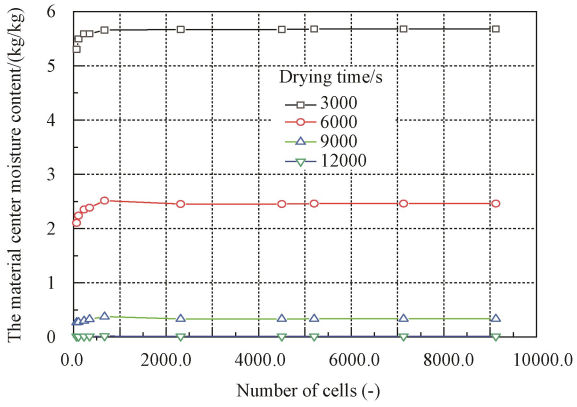

a. Changes in moisture content at the center of carrot slices

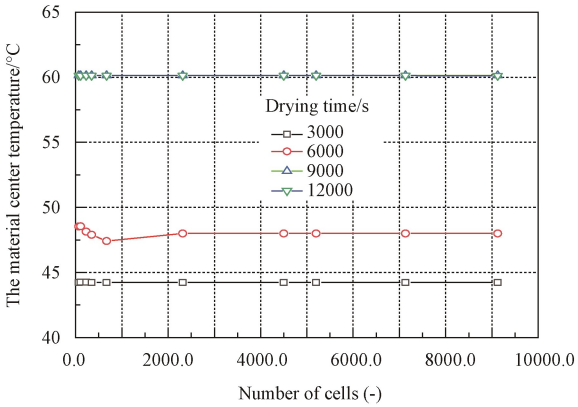

b. the changes in material temperature at the center of carrot slices

Figure 5 Influence of the cell number on the results of simulations of the drying of carrot slices at the temperature of 60°C, air velocity of 0.3 m/s, and RH of 20%

In order to validate the accuracy of the model, the experimental data obtained for the temperature and the moisture ratio of carrot slices during drying were compared with the computed data. The computed values (considering or neglecting shrinkage) and experimental data obtained for the moisture ratio and temperature of carrot slices during convective drying under the temperature of 60°C, air velocity of 0.3 m/s, and RH of 20% are shown in Figures 6a and 6b. Even with minor simulation errors found at the early stages of drying, the results show good agreement between the computed (with shrinkage) material temperature and moisture ratio of carrot slices and the experimental data (Figures 6a and 6b). The mean relative errors of simulations (considering shrinkage) of changes in moisture ratio and material temperature were 5.9% and 8.1%, respectively. The results prove that the Quadratic model fits well with the experimental data.

3.5 Comparison of model predictions with experimental data for material temperature and moisture ratio

A comparison of model predictions (considering shrinkage) with measurements for material temperature and moisture ratio of carrot slices is shown in Figs. 6c and 6d. The results show that the error of the simulation was lower than 10%. The drying time decreased and the drying rate increased when the drying temperature increased (Figure 6c). Initially, the computed values (shrinkage neglected) of the moisture ratio were smaller than the experimental ones. Then, the trend of predictions changed and finally, the computed values of the moisture ratio were much larger than the experimental ones. Most probably, the shrinkage of carrot slices significantly affected their porosity and hindered the moisture migration in the early stage of drying. Additionally, it reduced the moisture migration path and promoted moisture transfer in the later stages of the drying process. The results are consistent with published data[22].

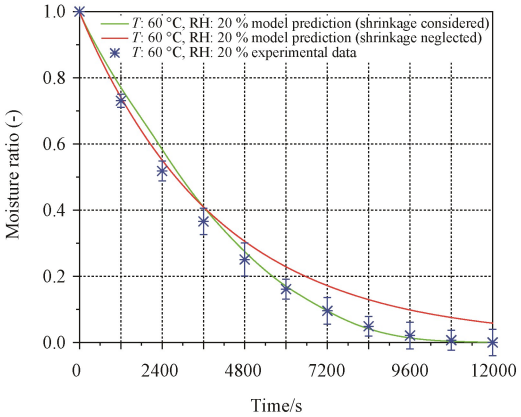

a. Changes in moisture ratio (temperature: 60°C, air velocity: 0.3 m/s, RH: 20%

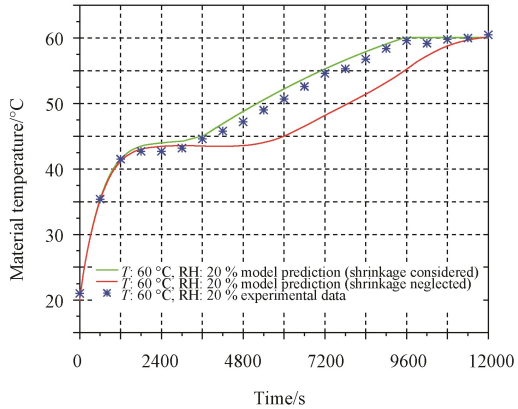

b. Changes in material temperature (temperature: 60°C, air velocity: 0.3 m/s, RH: 20%)

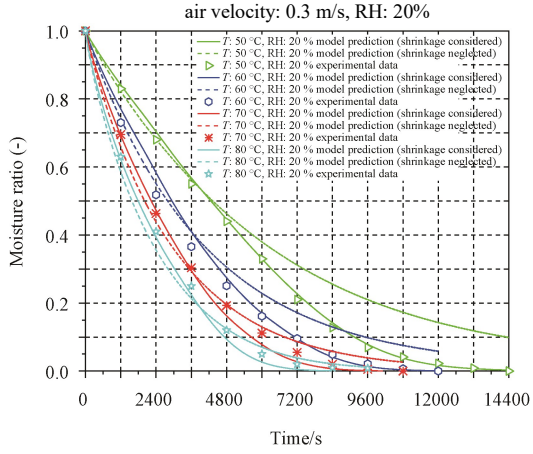

c. Changes in moisture ratio (temperature: 50°C, 60°C, 70°C, 80°C, air velocity: 0.3 m/s, RH: 20%)

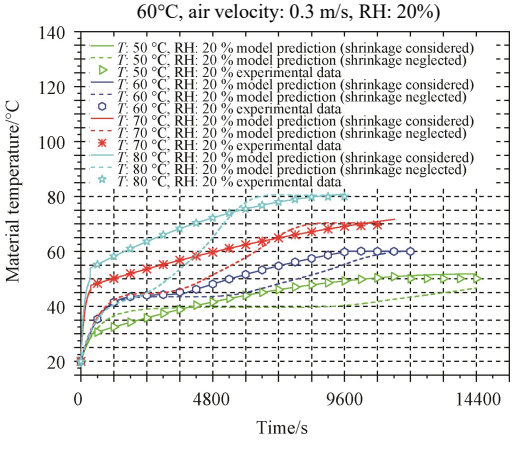

d. Changes in material temperature (temperature: 50°C, 60°C, 70°C, 80°C, air velocity: 0.3 m/s, RH: 20%)

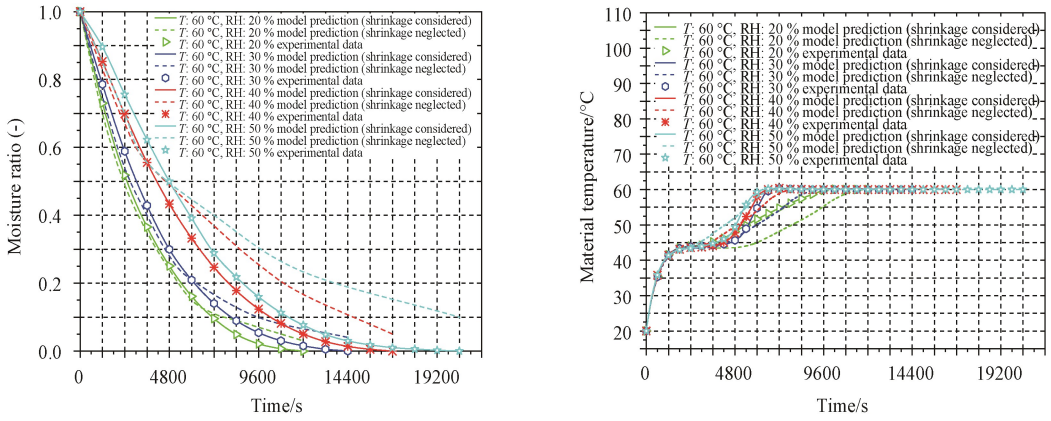

e. Changes in moisture ratio (temperature: 60°C, RH: 20%, 30%, 40%, 50%, air velocity: 0.3 m/s)

f. Changes in material temperature (temperature: 60°C, RH: 20%, 30%, 40%, 50%, air velocity: 0.3 m/s)

Figure 6 Results of model predictions (considering or neglecting shrinkage) and the experimental data obtained during convective drying of carrot slices

Similarly, the computed values (considering shrinkage) for material temperature and the experimental ones indicate a good fitting of the model to the experimental values obtained under different drying temperatures. The computed (considering shrinkage) material temperature reached the equilibrium temperature at the very beginning of drying and then increased slowly until the temperature close to that of the drying air. When the material temperature was computed without material shrinkage consideration, the computed equilibrium temperature of carrot slices was much lower than the experimental value in the early stage of drying. In the later stages of the drying process, a slow and finally rapid increase in the material temperature was observed (Figure 6c). The results can be explained by the fact that the moisture absorbed a large amount of heat and thus evaporated quickly in the early stage of drying resulting in a slow increase in the material temperature during drying. In the later stages of the drying process, it evaporated much slower and thus the material temperature increased more sharply.

The computed values (considering shrinkage) for material temperature and the experimental ones indicate a good fitting of the model to the experimental values measured under different RH of the drying air. The computed values (considering shrinkage) for material temperature were closer to the experimental ones compared to that computed without shrinkage consideration. The drying time decreased and the drying rate increased when the RH of the drying air decreased (Figure 6e). The driving force could increase with the decrease in RH of drying air as a result of the higher difference between the vapor pressure of surface water and the partial pressure of water vapor of the drying air[28]. The drying time was 12 000, 14 400, 16 800, and 20 400 s when hot air drying of carrot slices was conducted at the drying temperature of 60 °C and RH of the drying air of 20%, 30%, 40%, and 50%, respectively. The temperature of material dried under different RH of the drying air reached an equilibrium temperature rapidly at the very beginning of drying and then increased slowly until it reached a temperature close to that of the drying air. It can be clearly seen that the higher the RH of the drying air, the faster the increase in the temperature of the material to be dried (Figure 6f). For example, the temperature of material dried by the hot air of RH of 50% reached the temperature of the drying air 3600 s faster than that dried by the hot air of RH of 20%. The results can be explained by the fact that the reduced amount of heat absorbed by the moisture may result in slower moisture evaporation from the material dried by the hot air of high RH values[28]. Additionally, the higher RH of the drying air and thus the higher enthalpy of the drying medium may promote the increase in material temperature[28].

3.6 3D simulation of the moisture distribution and material temperature

The results of the simulation were compared with the experimental data to investigate the importance of the shrinkage phenomenon on the drying kinetics of carrot slices. The model was capable of predicting the changes in the temperature of the carrot slice with and without shrinkage of the sample. The changes in the temperature of material dried at the temperature of 80°C were predicted with and without shrinkage of the samples (Figure 7). It was found that they did not differ significantly at the very beginning of drying, i.e., after 120 s of the drying process. The importance of the shrinkage phenomenon on the drying kinetics of carrot slices was not obvious when only the initial drying period was taken into consideration. The trend of changes in the material temperature within the first 120 s of the drying process was quite similar to that without shrinkage. The results indicate that the temperature at the surface of the carrot slice was 26°C, while the temperature in the center of the dried particle was 23°C. As the drying time increased, the material temperature predicted with the model taking into account material shrinkage was even 10°C higher than that predicted by the model without shrinkage consideration (Figure 6d). The results show that shrinkage led to a decrease in the sample volume. The shrinkage phenomenon accelerated heat conduction from the material surface to the center of the sample and thus resulted in the rapid increase in material temperature. The material temperature predicted with the model considering shrinkage was about 8°C higher than that predicted by the model without shrinkage consideration. It was found that the material temperature computed with the model considering shrinkage approached the drying air temperature much faster than that predicted by the model without shrinkage consideration. Additionally, the results show that material shrinkage significantly influenced heat conduction. The material temperature predicted with the model considering shrinkage was much closer to the measured values than that

predicted by the model without shrinkage consideration. It should be also pointed out that the material shrinkage did not significantly affect the temperature distribution inside the carrot slice during drying.

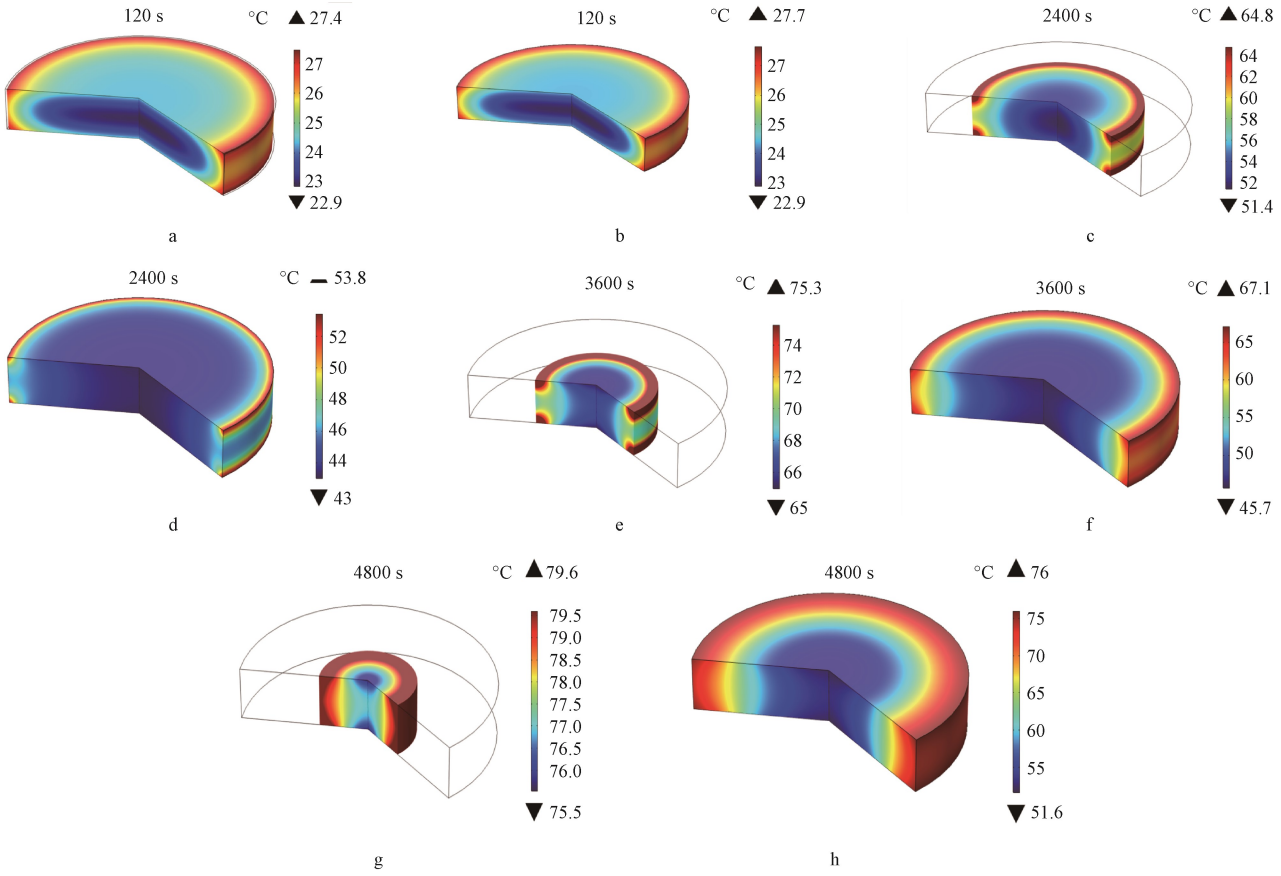

a, c, e, and g: the 3D model of temperature distribution in carrot slice with shrinkage considered b, d, f, and h: the 3D model of temperature distribution in carrot slice with shrinkage neglected. The results of simulations at different time intervals: a and b: 120 s; c and d: 2400 s; e and f: 3600 s; g and h: 4800 s.

Figure 7 3D model of temperature distribution in carrot slice during hot air drying at the temperature of 80°C, air velocity of 0.3 m/s, RH of 20%

The model was also capable of predicting the changes in moisture content of carrot slices with and without shrinkage of the sample (Figure 8). The 3D model of moisture distribution in carrot slices during hot air drying at the temperature of 80°C, air velocity of 0.3 m/s, and RH of 20% is shown in Figure 8. The results show that the moisture content in the center of the dried particle was much higher than that on its surface. The moisture content at the material surface predicted with the model considering shrinkage decreased much faster than that predicted without shrinkage. As the drying time progressed, the moisture inside the material was moved towards its surface, while the surface moisture content was maintained in equilibrium with the moisture content of the drying air. Even after 480 s of drying, the moisture content inside the dried particle was 0.93 kg/kg, while that on its surface was 0.25 kg/kg. The results indicate a large moisture gradient inside the dried material even after quite a long drying time. As the drying time progressed from 120 s to 3600 s, the moisture content predicted with the model considering shrinkage was higher than that predicted without shrinkage consideration. However, after 4800 s of drying, the trend of changes in moisture content predicted with the model considering shrinkage was lower than that predicted without shrinkage consideration. It can be explained by the fact that shrinkage of carrot slices significantly affected their porosity and thus hindered the moisture migration at the very early stages of drying. In the later stages of the drying process, shrinkage reduced the moisture migration path and promoted moisture transfer (Figures 6c and 6d). The results are consistent with the published data[22,33].

The model was capable of predicting the 3D temperature distribution of carrot slices during drying with an air of different RH values (Figure 9). The temperature of material dried by the air of RH of 50% increased much faster than that dried by the air of RH of 20% as the drying time increased to 7200 s (Figure 6f). After 720 s of drying, the temperatures of materials dried by the air of RH of 20 and 50% were found to be almost the same. However, the results of this study show that the shrinkage rate of carrot slices dried by the air of RH of 20% was much higher than that dried by the air of RH of 50% (Figure 4). It can be explained by the fact that the rapid evaporation of moisture increased the thermal and moisture stresses resulting in high shrinkage values. The results are consistent with published data[33]. As shown in Figure 10, after the same drying time, the moisture content of material dried by the air of RH of 50% RH was significantly higher than that dried by the air of RH of 20% (Figures 6e and 6f). The results indicate that the higher the relative humidity of the drying air was, the longer the drying time. It can be explained by the fact that the small difference between the water vapor partial pressure at the sample surface and the drying air did not promote moisture evaporation. The results are consistent with published data[28,34].

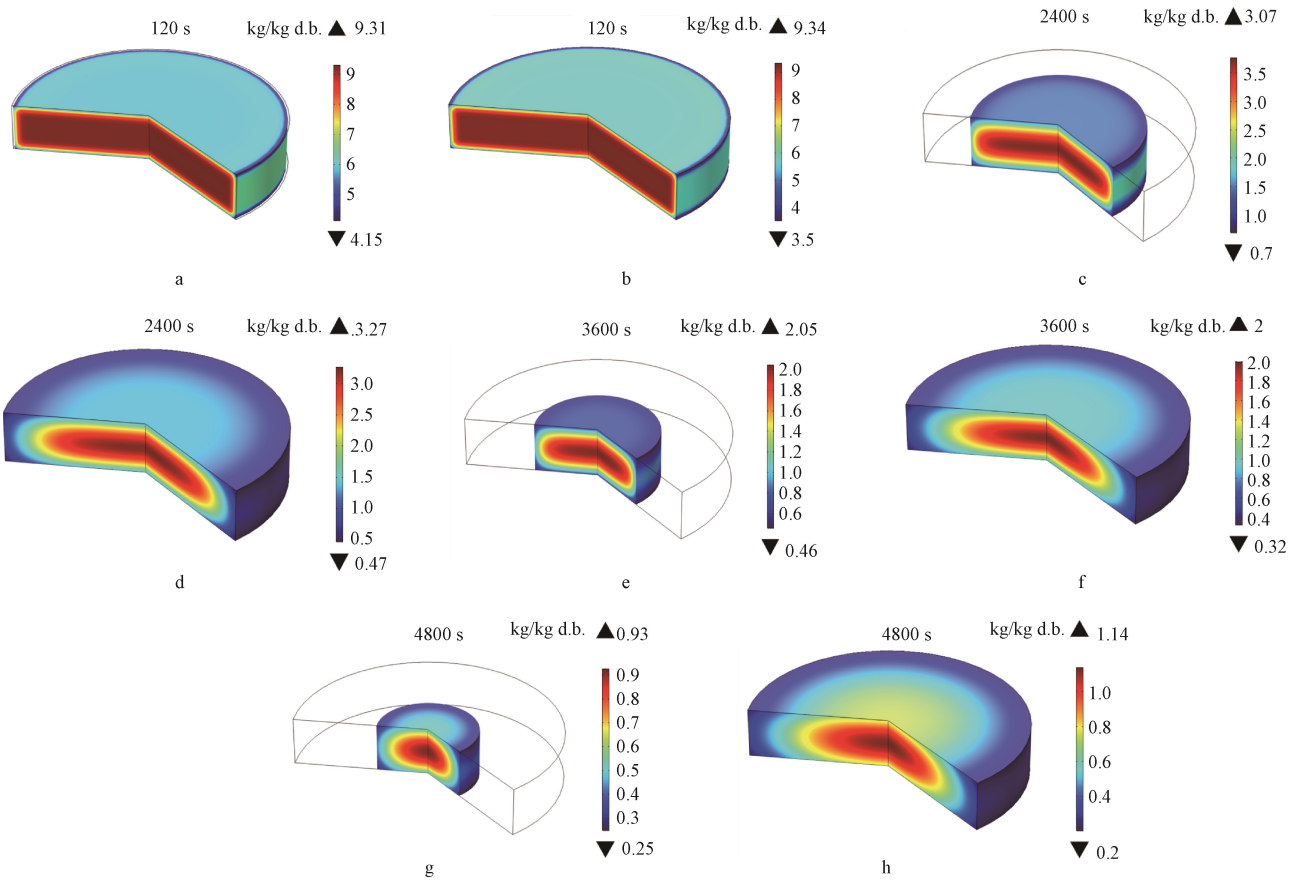

a, c, e, and g: the 3D model of moisture distribution in carrot slice (shrinkage considered); b, d, f, and h: the 3D model of moisture distribution in carrot slice (shrinkage neglected). The results of simulations at different time intervals: a and b: 120 s; c and d: 2400 s; e and f: 3600 s; g and h: 4800 s.

Figure 8 3D model of moisture distribution in carrot slice during hot air drying at the temperature of 80°C, air velocity of 0.3 m/s, RH of 20%

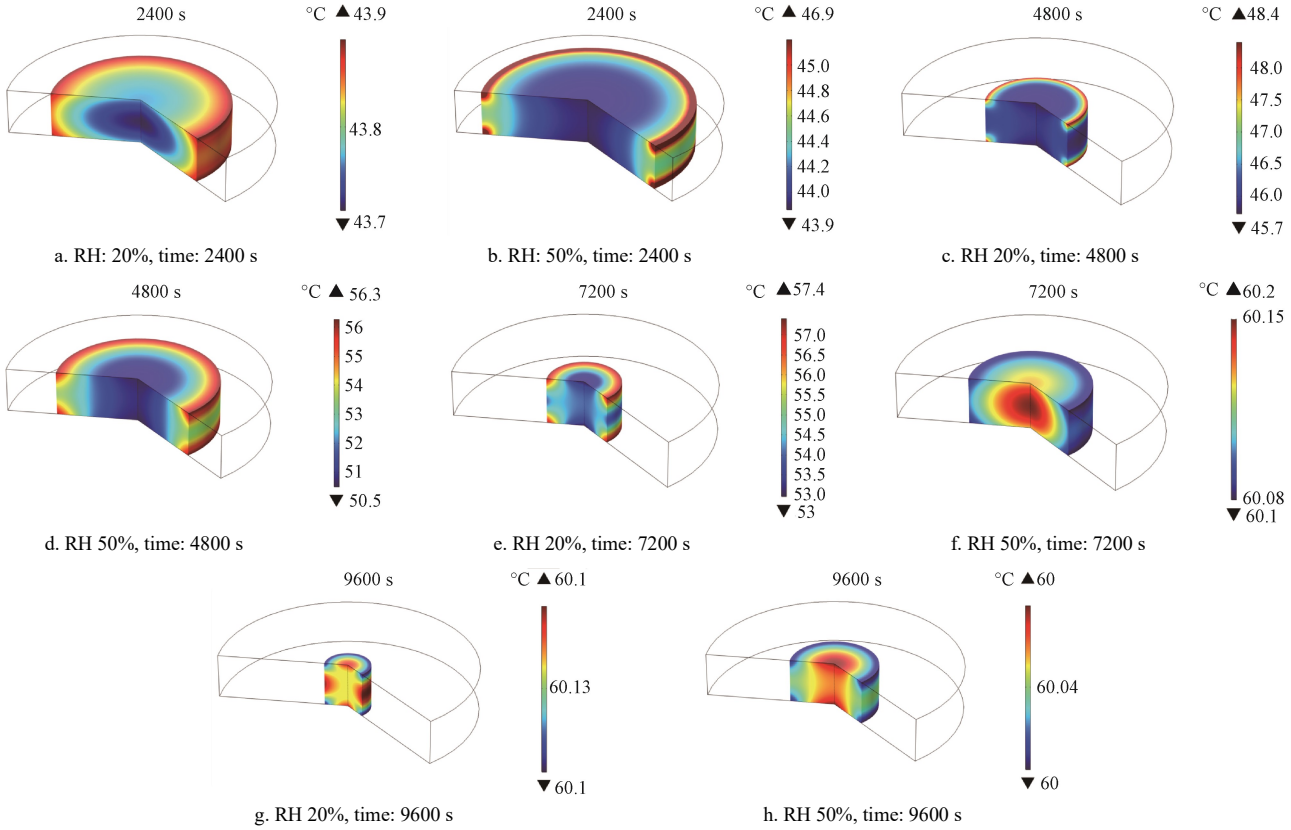

Figure 9 3D model (with shrinkage considered) of temperature distribution in carrot slice during hot air drying at the temperature of 60°C, air velocity of 0.3 m/s, RH of 20 and 50%

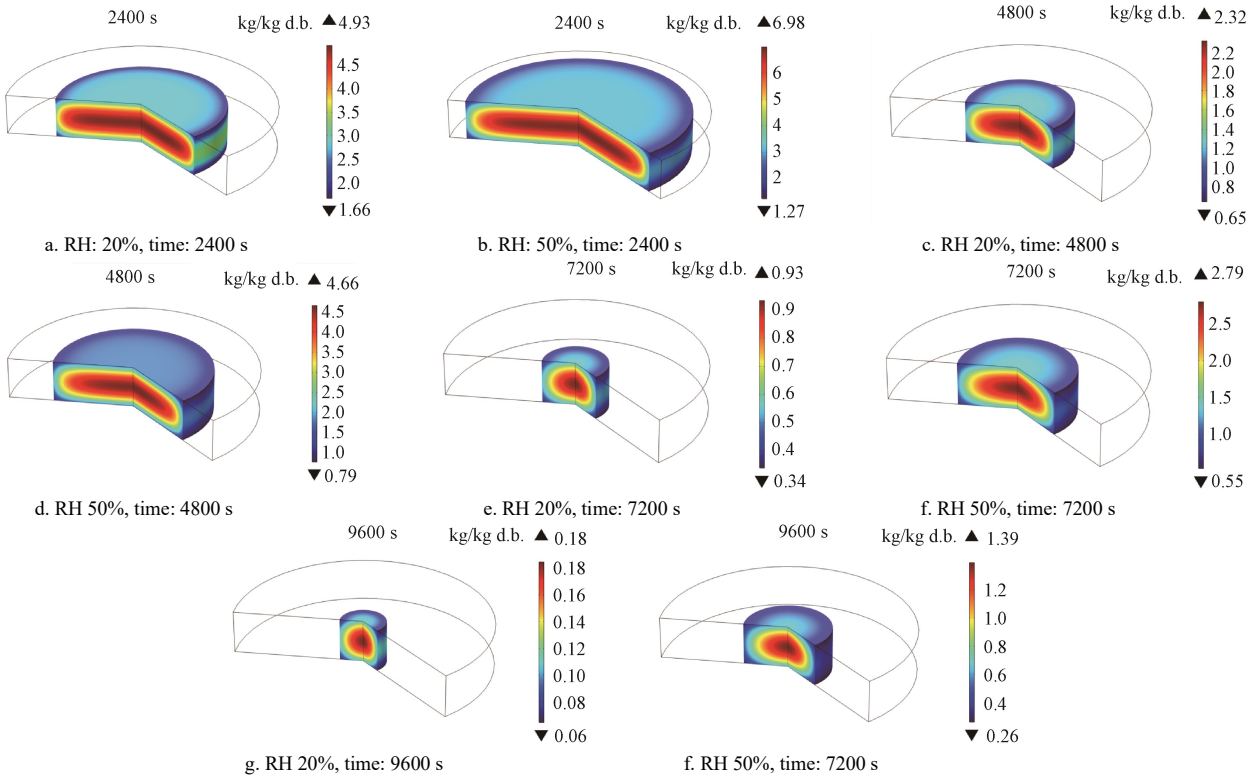

Figure 10 3D model (with shrinkage considered) of moisture distribution in carrot slice during hot air drying at the temperature of 60°C, air velocity of 0.3 m/s, RH of 20 and 50%

4 Conclusions

In this study, numerical simulations (considering or neglecting shrinkage) of heat and mass transfer in convective drying of carrot slices under constant and controlled temperature and relative humidity were carried out. The results show that the model fitted well to the moisture ratio and the material temperature data changing trend with average relative errors of 5.9% and 8.1%, respectively. The significant findings of this study are as follows:

1) Temperature and relative humidity significantly affected the volume shrinkage of carrot slices. The volume shrinkage increased with the rising of the constant temperature and the decline of relative humidity. The material moisture content was significantly related to the shrinkage of dried tissue.

2) The Quadratic model fitted well to the experimental data (R^2>0.99) and it was selected to simulate the relationship between volume shrinkage and moisture ratio under constant drying conditions.

3) The results of the simulation considering shrinkage show that the moisture and temperature distributions during drying were closer to the experimental data than the results of the simulation disregarding shrinkage.

This model can be used to provide more information on the dynamics of heat and mass transfer during drying and can also be adapted to other products and dryers devices. This finding may help optimize the drying process to reduce the material structure change.

Nomenclature

Symbol	Meaning/Unit
A_w	Water activity
A	Empirical coefficient of contraction
B	Empirical coefficient of contraction
C	Empirical coefficient of contraction
C_p	Specific heat, J/kg·K
D_{AB}	Diffusivity of water vapor in air, m^2/s
D_{eff}	Effective moisture diffusivity, m^2/s
d_E	Average diameter of volume, m
h_{air}	Specific enthalpy of wet air, J/kg
h_m	Mass transfer coefficient, m/s
h_t	Heat transfer coefficient, W/m^2·K
I	Irreversible
K	Thermal conductivity, W/m·K
M	Moisture content, (kg/kg, dry basis)
MR	Moisture ratio
Nu	Nusselt number
Pr	Prandtl number
P_s	Saturated water vapor pressure at surface, Pa
r_0	Material initial radius, m
r_w	Latent heat of water evaporation, J/kg
Re	Reynolds number
RH	Relative humidity, %
Sc	Schmidt number
Sh	Sherwood number
T	Operation time, s
T	Material temperature, K
T_0	Initial material temperature, K
Ts	Material surface temperature, K
V	Air velocity, m/s
v_{SR}	Shrinkage rate, m/s
M_t	Moisture content at any time, (kg/kg d.b., dry base)
W_t	Material mass at any time, kg
WC	Concentration of water vapor, kg/m^3
G	Mass of a dry matter, kg
M_0	Initial moisture content, (kg/kg d.b., dry basis)
SR_t	Thickness shrinkage at drying time of t, %
TH_t	Sample thickness at any time t during drying, m
TH_0	Initial sample thickness, m
SR_d	Cross-sectional shrinkage, %
d_t	Cross-sectional diameter of the sample at any time t, m
d_0	Initial cross section diameter of a sample, m
SR_v	Volume shrinkage, %
t_1	Drying time, s
t_2	Drying time, s
SR_{t1}	Thickness shrinkage at drying time of t_1, %
SR_{t2}	Thickness shrinkage at drying time of t_2, %
SRR_t	Rate of thickness shrinkage, (1/s)

SR_{df1}	Cross-sectional shrinkage at the drying time t_1, %
SR_{df2}	Cross-sectional shrinkage at the drying time t_2, %
SR_{Vf1}	Volume shrinkage at the drying time t_1, %
SR_{Vf2}	Volume shrinkage at the drying time t_2, %
SRR_d	Rate of cross-sectional shrinkage, (1/s)
SRR_V	Rate of volume shrinkage, (1/s)
P	Material density, kg/m^3
ρ_w	Water density, kg/m^3
Λ	Air conductivity, W/m·K
M	Viscosity, Pa·s
Subscripts	
air	Air
dry	Drying air
e	Exhaust air
h	Heating material
In	Input
m	Material
out	Output
ref	Reference state
s	Surface
w	Water

Acknowledgements

This study was financially supported by Earmarked Fund for China Agriculture Research System (CARS-21).

[References]

[1] Yu X L, Zielinska M, Ju H Y, Mujumdar A S, Duan X, Gao Z J, et al. Multistage relative humidity control strategy enhances energy and exergy efficiency of convective drying of carrot cubes. International Journal of Heat and Mass Transfer, 2020; 14(9): 119231. doi: 10.1016/j.ijheatmasstransfer.2019.119231.

[2] Karim M A, Hawlader M N A. Mathematical modelling and experimental investigation of tropical fruits drying. International Journal of Heat and Mass Transfer, 2005; 48(23-24): 4914–4925. doi: 10.1016/j.ijheatmasstransfer.2005.04.035.

[3] Khan M I H, Wellard R M, Nagy S A, Joardder M U H, Karim M A. Investigation of bound and free water in plant-based food material using NMR T-2 relaxometry. Innovative Food Science & Emerging Technologies, 2016; 38(PartA): 252–261.

[4] Srikiatden J, Roberts J S. Predicting moisture profiles in potato and carrot during convective hot air drying using isothermally measured effective diffusivity. Journal of Food Engineering, 2008; 84(4): 516–525.

[5] Khan M I H, Karim M A. Cellular water distribution, transport, and its investigation methods for plant-based food material. Food Research International, 2017; 99(Part1): 1–14.

[6] Mayor L, Sereno A M. Modelling shrinkage during convective drying of food materials: A review. Journal of Food Engineering, 2004; 61(3): 373–386.

[7] Vincent J F V. Relationship between density and stiffness of apple flesh. Journal of the Science of Food and Agriculture, 1989; 47(4): 443–462.

[8] Senadeera W, Bhandari B.R, Young G, Wijesinghe B. Modeling dimensional shrinkage of shaped foods in fluidized bed drying. Journal of Food Processing and Preservation, 2005; 29(2): 109–119.

[9] Aprajeeta J, Gopirajah R, Anandharamakrishnan C. Shrinkage and porosity effects on heat and mass transfer during potato drying. Journal of Food Engineering, 2015; 14(4): 119–128.

[10] Pacheco-Aguirre F M, Garcia-Alvarado M A, Corona-Jimenez E, Ruiz-Espinosa H, Cortes-Zavaleta O, Ruiz-Lopez I I. Drying modeling in products undergoing simultaneous size reduction and shape change: Appraisal of deformation effect on water diffusivity. Journal of Food Engineering, 2015; 16(4): 30–39.

[11] Pandit R B, Prasad S. Finite element analysis of microwave heating of potato-transient temperature profiles. Journal of Food Engineering, 2003; 60(2): 193–202.

[12] Srikiatden J, Roberts J S. Measuring moisture diffusivity of potato and carrot (core and cortex) during convective hot air and isothermal drying. Journal of Food Engineering, 2006, 74(1): 143–152.

[13] Aversa M, Curcio S, Calabro V, Iorio G. An analysis of the transport phenomena occurring during food drying process. Journal of Food Engineering, 2007; 78(3): 922–932.

[14] Curcio S, Aversa M, Calabro V, Iorio G. Simulation of food drying: FEM analysis and experimental validation. Journal of Food Engineering, 2008; 87(4): 541–553.

[15] Wang N, Brennan J G. A mathematical-model of simultaneous heat and moisture transfer during drying of potato. Journal of Food Engineering, 1995; 24(1): 47–60.

[16] Yang H, Sakai N, Watanabe M. Drying model with non-isotropic shrinkage deformation undergoing simultaneous heat and mass transfer. Drying Technology, 2001; 19(7): 1441–1460.

[17] Gulati T, Datta A K. Mechanistic understanding of case-hardening and texture development during drying of food materials. Journal of Food Engineering, 2015; 16(6): 119–138.

[18] Jomaa W, Puiggali J R. Drying of shrinking materials - modelings with shrinkage velocity.Drying Technology, 1991; 9(5): 1271–1293.

[19] Segura L A, Badillo G M, Alves-Filho O. Microstructural changes of apples (Granny Smith) during drying: visual microstructural changes and possible explanation from capillary pressure data. Drying Technology, 2014; 32(14): 1692–1698.

[20] Silva V, Costa J J, Rui Figueiredo A, Nunes J, Nunes C, Ribeiro T I B, et al. Study of three-stage intermittent drying of pears considering shrinkage and variable diffusion coefficient. Journal of Food Engineering, 2016; 18(6): 77–86.

[21] Tao Y, Li D D, Chai W S, Show P L, Yang X H, Manickam S, et al. Comparison between airborne ultrasound and contact ultrasound to intensify air drying of blackberry: Heat and mass transfer simulation, energy consumption and quality evaluation. Ultrasonics Sonochemistry, 2021; 72: 105410. doi: 10.1016/j.ultsonch.2020.105410.

[22] Association of Official Analytical Chemists (AOAC). Official method of analysis association of official analytical chemists, 15th ed. Washington DC: AOAC International Publisher, 1990; 1024p.

[23] Li X Y, Liu Y H, Gao Z J, Xie Y K, Wang H. Computer vision online measurement of shiitake mushroom (*Lentinus edodes*) surface wrinkling and shrinkage during hot air drying with humidity control. Journal of Food Engineering, 2021; 292: 110253. doi: 10.1016/j.jfoodeng.2020.110253.

[24] Suvarnakuta, P, Devahastin, S, Mujumdar, A S. A mathematical model for low-pressure superheated steam drying of a biomaterial. Chemical Engineering and Processing: Process Intensification, 2007; 46(7): 675–683.

[25] Bai J W, Tian X Y, Liu Y J, Xu S R, Luo H. Studies on drying characteristics and shrinkage kunetics modelling of *Colocasia gigantea* slices during thin layer drying. Journal of Chinese Institute of Food Science and Technology, 2018; 18(8): 1009–1848.

[26] Air-Conditioning and Heating Systems. In: 2012 ASHRAE handbook: Heating, ventilating, and air-conditioning systems and equipment. SI Ed, 2012; 1.1–1.18.

[27] Ruiz-Lopez I I, Cordova A V, Rodriguez-Jimenes G C, Garcia-Alvarado M A. Moisture and temperature evolution during food drying: Effect of variable properties. Journal of Food Engineering, 2004; 63(1): 117–124.

[28] Pauli M, Kayser T, Adamiuk G, Wiesbeck W. Modeling of mutual coupling between electromagnetic and thermal fields in microwave heating. In: 2007 IEEE/MTT-S International Microwave Symposium, Honolulu: IEEE, 2007; 1983-1986. doi: 10.1109/MWSYM.2007.380201.

[29] Ju H Y, Zhao S H, Mujumdar A S, Zhao H Y, Duan X, Zheng Z A, et al. Step-down relative humidity convective air drying strategy to enhance drying kinetics, efficiency, and quality of American ginseng root (*Panax quinquefolium*). Drying Technology, 2020; 38(7): 903–916.

[30] Xie J, Gao Z J. Study on adaptability of hot air drying technology based on temperature and humidity control for fruit and vegetable materials drying. Agricultural Science and Engineering in China, 2019; 31(1): 37–48.

[31] Tzempelikos D A, Mitrakos, D, Vouros A P, Baardakas A V, Filios A E, Margaris D P. Numerical modeling of heat and mass transfer during convective drying of cylindrical quince slices. Journal of Food Engineering, 2015; 15(6): 10–21.

[32] Jin H H, Li W F, Xiao X L. Drying characteristics and model of banana in air-impingement jet dryer. Farm Products Processing, 2015; 1(3): 1671–9646.

[33] Ratti C. Shrinkage during drying of foodstuffs. Journal of Food Engineering, 1994; 23(1): 91–105.

[34] Yuan Y J, Tan L B, Xu Y Y, Yuan Y D, Dong J X. Numerical and experimental study on drying shrinkage-deformation of apple slices during process of heat-mass transfer. International Journal of Thermal Sciences, 2019; 136: 539–548.